Regulation of Mitochondrial Fragmentation in Microvascular Endothelial Cells Isolated from the SU5416/Hypoxia model of Pulmonary Arterial Hypertension

Karthik Suresh[1], Laura Servinsky[1], Haiyang Jiang[1], Zahna Bigham[1], Joel Zaldumbide[1], John C. Huetsch[1], Corrine Kliment[1], Michelle G. Acoba[2], Brian J. Kirsch[3], Steven M. Claypool[2], Anne Le[3], Mahendra Damarla[1], and Larissa A. Shimoda[1]

[1] Division of Pulmonary and Critical Care Medicine, Department of Medicine, Johns Hopkins University School of Medicine, Baltimore, MD 21224

[2] Department of Physiology, Johns Hopkins University School of Medicine, Baltimore, MD 21205

[3] Department of Pathology, Johns Hopkins University School of Medicine, Baltimore, MD 21205

Running title: mtROS and fragmentation in SuHx MVECs

Address for Correspondence:

Karthik Suresh, MD

Johns Hopkins Asthma and Allergy Building

5501 Hopkins Bayview Circle

Baltimore, MD 21224

Phone: 410-550-4158

FAX:410-550-2612

Email: ksuresh2@jhmi.edu

Abstract

Pulmonary arterial hypertension (PAH) is a morbid disease characterized by progressive right ventricle (RV) failure due to elevated pulmonary artery pressures (PAP). In PAH, histologically complex vaso-occlusive lesions in the pulmonary vasculature contribute to elevated PAP. However, the mechanisms underlying dysfunction of the microvascular endothelial cells (MVECs) that comprise a significant portion of these lesions are not well understood. We recently showed that MVECs isolated from the rat Sugen/Hypoxia (SuHx) experimental model of PAH (SuHx-MVECs) exhibit increases in: migration/proliferation, mitochondrial ROS (mtROS) production, intracellular calcium levels ($[Ca^{2+}]_i$) and mitochondrial fragmentation. Furthermore, quenching mtROS with the targeted antioxidant MitoQ attenuated basal $[Ca^{2+}]_i$, migration and proliferation; however, whether increased mtROS-induced $[Ca^{2+}]_i$ entry affected mitochondrial morphology was not clear. In this study, we sought to better understand the relationship between increased ROS, $[Ca^{2+}]_i$ and mitochondrial morphology in SuHx-MVECs. We measured changes in mitochondrial morphology at baseline and following inhibition of mtROS, with the targeted antioxidant MitoQ, or transient receptor potential vanilloid-4 (TRPV4) channels, which we previously showed were responsible for mtROS-induced increases in $[Ca^{2+}]_i$ in SuHx-MVECs. Quenching mtROS or inhibiting TRPV4 attenuated fragmentation in SuHx-MVECs. Conversely, inducing mtROS production in MVECs from normoxic rats (N-MVECs) increased fragmentation. Ca^{2+} entry induced by the TRPV4 agonist, GSK1017920A, was significantly increased in SuHx-MVECs and was attenuated with MitoQ treatment, indicating that mtROS contributes to increased TRPV4 activity in SuHx-MVECs. Basal and maximal respiration were depressed in SuHx-MVECs, and inhibiting mtROS, but not TRPV4, improved respiration in these cells. Collectively, our data show that, in SuHx-MVECs, mtROS production promotes: a) TRPV4-mediated increases in $[Ca^{2+}]_i$; b) mitochondrial fission and c) decreased mitochondrial respiration. These results suggest an important role for mtROS in driving MVEC dysfunction in PAH.

Introduction

In pulmonary arterial hypertension (PAH), progressive increases in pulmonary artery pressure lead to right ventricular dysfunction, failure and eventually death. Endothelial cell (EC) dysfunction is thought to contribute to vaso-occlusive lesion formation and increased pulmonary artery pressures in PAH. For instance, ECs in PAH patients exhibit increased proliferation and evidence of oxidant stress (12). The hyper-proliferative ECs in PAH are thought to be of microvascular origin, referring to ECs that originate from the small diameter vessels in the lung (46). Similar to what is observed *in vivo*, ECs isolated from human lungs with PAH also exhibit exuberant growth capacity, with increased migration and proliferation *in vitro* (18, 75-77). However, the mechanisms underlying the changes seen in PAH ECs, such as increased migration and proliferation *in vivo* and *in vitro*, are not fully understood.

In order to better understand the pathobiologic mechanisms of EC dysfunction in PAH, we recently isolated microvascular ECs (MVECs) from the Sugen/Hypoxia (SuHx) rat model of experimental PAH (53). In this model, rats are given a one-time injection of SU5416, a vascular endothelial growth factor receptor-2 (VEGFR2) inhibitor, and placed in hypoxia for three weeks, followed by return to normoxia. As shown by numerous labs (29, 39, 62), SuHx rats exhibit hemodynamic and histologic changes, including increased right ventricular systolic pressure (RVSP) and presence of vaso-occlusive lesions, similar to human PAH (12).

Using MVECs isolated from normoxic (N-MVECs) and SuHx (SuHx-MVEC) rats, we recently observed evidence of endothelial-to-mesenchymal transition (EndMT), a process associated with an oncogenic cell phenotype characterized by increased migration, proliferation and metabolic changes such as glycolytic shift (19, 35, 57). EndMT, increased migration and proliferation in ECs have been noted by other labs using various PAH models (57, 60, 73). To determine the mechanistic basis for these functional changes, we measured reactive oxygen species (ROS) and intracellular calcium concentration ($[Ca^{2+}]_i$) levels, signaling molecules that play key roles in promoting migration and proliferation in EC (2, 20, 61, 65). We found that baseline ROS levels and $[Ca^{2+}]_i$ were both increased in SuHx-MVEC (53), and that SuHx-MVEC ROS levels were normalized by quenching mitochondrial ROS (mtROS), while basal $[Ca^{2+}]_i$ was attenuated by inhibiting either mtROS or the Ca^{2+} channel, transient receptor potential vanilloid-4 (TRPV4) (53), suggesting a possible mechanistic link

between mtROS production and TRPV4 activation in SuHx-MVEC. Furthermore, inhibiting either mtROS or TRPV4 similarly attenuated migration and proliferation in SuHx-MVEC. Collectively, these data suggested a link between mtROS and $[Ca^{2+}]_i$ in facilitating SuHx-MVEC migration and proliferation, although the exact interactions between these two pathways remains incompletely understood.

As part of our study of mtROS in SuHx-MVECs, we recently examined mitochondrial structure and function and observed increased fragmentation (53). Mitochondrial dysfunction has been extensively studied in pulmonary artery smooth muscle cells (PASMCs) in PAH; for instance, a distinct role for mitochondrial dysfunction in promoting PASMC dysfunction has been previously established (5-7, 11, 37, 49, 64). Similar to PASMCs, mitochondrial dysfunction has been observed in ECs isolated from humans with PAH (77), but unlike in PASMCs, the mechanistic details underlying mitochondrial dysfunction in MVEC are still under investigation.

In PASMCs, one critical aspect of mitochondrial dysfunction is the dysregulation of mitochondrial fission/fusion dynamics (5, 44). Mitochondria are dynamic organelles that constantly undergo fission (i.e. fragmentation) and fusion. At baseline, fission and fusion are in equilibrium. However, a shift in the balance between fusion and fission can occur in situations of cellular stress (44). Interestingly, though increases in fission and mtROS production often occur together (32), the mechanistic links connecting mtROS production to changes in mitochondrial morphology are not fully known, particularly in ECs. Similarly, increased $[Ca^{2+}]_i$ is associated with mitochondrial dysfunction in a variety of cell types (16, 28, 31, 43) but the specific effect of changes in cytosolic Ca^{2+} on mitochondrial morphology in vascular ECs has not been fully resolved.

In addition to increased levels of ROS and $[Ca^{2+}]_i$, changes in mitochondrial morphology can also be induced by shifts in mitochondrial bioenergetics. For instance, a shift towards fatty acid oxidation is associated with both increased fragmentation (48, 52) and fusion (33), depending on the cell type. Previously, we found that basal and maximal oxygen consumption rate (OCR) were decreased in SuHx-MVECs, while extracellular acidification rate (ECAR) was increased, suggestive of a glycolytic shift in the mitochondrial energetic profile (53) similar to that observed in cancer cells and other cell types with high migratory/proliferative capacity (70) including human PAH ECs (75). Taken together, our prior oxidative phosphorylation and mitochondrial fragmentation data reinforced the hypothesis that significant mitochondrial dysfunction was present in SuHx-

MVECs. However, the role played by elevated $[Ca^{2+}]_i$, and the interaction between mtROS and $[Ca^{2+}]_i$, in regulating mitochondrial dynamics and energetics remain unknown. Thus, we hypothesized that mtROS production activates TRPV4 and increases $[Ca^{2+}]_i$ in SuHx-MVECs, promoting fragmentation. We reasoned that this feed-forward mechanism might explain increased basal levels of mitochondrial fragmentation, mtROS and $[Ca^{2+}]_i$ in SuHx-MVEC maintained in culture, even in the absence of exogenous injurious agonists. Thus, in this study, we measured the effect of changing mtROS or $[Ca^{2+}]_i$ on mitochondrial structure (i.e. morphology) and function (i.e. respiration) in N- and SuHx-MVECs to determine the mechanistic links by which mtROS and $[Ca^{2+}]_i$ may be contributing to mitochondrial dysfunction.

Methods

All procedures were performed in accordance with the *NIH Guide for the Care and Use of Laboratory Animals,* and were approved by the Animal Care and Use Committee of The Johns Hopkins University School of Medicine.

Drugs and reagents: SU5416 was obtained from Tocris. Baculoviral constructs for MitoRFP and roGFP were obtained from Life Technologies. Antimycin A was obtained from Abcam. MitoQ (MQ) was provided by Antipodean Pharmaceuticals. GSK2193874 (GSK2) was obtained from SelleckChem, and HC-067047 (HC) was obtained from EMD Millipore. Cyclosporine A (CSA) was obtained from Sigma. Drug treatment times were 1h (GSK2, MQ, HC), 20 minutes (AA) or 30 minutes (CSA).

PAH animal model: Induction of the SuHx model was performed by injecting SU5416 prepared in a carboxymethylcellulose (CMC)-containing diluent as described earlier (29). Rats (male, Wistar, 250-350g, 4 month old) were injected with 20 mg/kg of SU5416 subcutaneously, then exposed to 10% hypoxia for three weeks before being returned to normoxia for two additional weeks. Control rats were injected with vehicle and maintained at room air for five weeks. All animals were kept in the same room, and thus were exposed to the same light/dark cycles and room temperatures. Animals were housed in standard rat cages at three rats per cage. No breeding was performed.

Hemodynamics: Following induction of anesthesia (i.p. pentobarbital sodium - 43 mg/kg) and confirmation (via paw pinch) of sufficient sedation depth, right ventricular systolic pressure (RVSP) measurements were made using a transdiapragmatic approach as previously described (29, 53). Animals were sacrificed (via exsanguination) after hemodynamic measurement and before the start of MVEC isolation.

Isolation and culture of MVEC: MVECs were isolated, grown to confluence and phenotyped at each passage as described previously (53, 55). Briefly, after hemodynamic measurements were made, peripheral strips of rat lung were dissected and digested with collagenase (type 1A; 1 mg/mL) dissolved in a DMEM-based media

containing 20% fetal bovine serum (FBS; Hyclone). Following digestion, cells were incubated with CD31-conjugated dynabeads (Invitrogen), magnetically selected, grown to confluence and then re-selected using *Griffonia simplicifolia*-conjugated beads (Vector). Following dual-selection, cells were again phenotyped for smooth muscle (smooth muscle actin, myosin heavy chain) and EC (von willebrand factor, *Griffonia* lectin) markers prior to being frozen at passage 3. All experiments were performed on cells at passage 3-4. All cells were grown in DMEM media containing antibiotics, endothelial growth factor supplement (Millipore) and 5% FBS as described previously (53).

Western Blotting: Confluent flasks of N- and SuHx-MVEC were trypsinized, pelleted and lysed with lysis buffer (T-PER) containing protease inhibitor cocktail tablet (Roche). Protein levels were quantified using a BCA kit (Pierce). Electrophoresis of equal amounts of protein was performed prior to transfer to PVDF membranes, blocking (5% BSA in TBS-T), incubation with primary antibody (phospho-Drp1, total Drp1 and Mfn-2: CST, 1:2000, overnight 4ºC) and appropriate secondary (goat anti-rabbit or anti-mouse: KPL, 1:10000, 1 h, RT) and ECL (Amersham, 3 minutes). Membranes were then stripped and re-probed for GAPDH (GAPDH-HRP: Bio-Rad, 1:10000).

Antibody Validation: We have previously provided full-length gels and validation information for the phosphor- and total Drp1 antibodies (pSer616: Cell Signaling #3455Ss; total Drp1: Cell Signaling #8570) (53). The Mfn-2 antibody used in this study (Cell Signaling, #9482) has been previously validated using siRNA (38). We have also provided a representative full-length Mfn-2 immunoblot lane in Supplemental Figure S1 (supplemental data available at: https://github.com/suresh-lab/mtMorph-TRPV4)

Mitochondrial morphology: Mitochondrial morphology measurements were made on semi-confluent monolayers of cells seeded on glass coverslips for 24 h in DMEM media with 5% FBS. Cells were incubated with Mitotracker (100 nM) for 20 minutes prior to being imaged on an Olympus fluorescence microscope (40x oil, frame rate: 5 frames/minute). All images were obtained under identical image conditions (light intensity, binning, gain, and magnification). Image processing was performed using an automated algorithm as recently described (53). Briefly, images of individual cells stained for mitochondria were analyzed using an automated image processing algorithm as described recently by Ouellet et al (41). After background subtraction, binning

and threshold were automatically determined prior to determination of mitochondrial network length using the Momito program. Output mitochondrial length distributions were collected and processed in R(45).

Oxygen consumption measurements: N- and SuHx-MVEC (20,000 cells/well) were plated on a XF96 V3 PS cell culture microplate and incubated overnight in DMEM containing 5% serum. The cells were then washed, incubated with base media (Agilent) containing: glutamine, pyruvate and glucose as described previously (53). Cells and treatment solutions (2 μM Oligomycin, 0.5 μM FCCP and 0.5 μM Rotenone/Antimycin A) were loaded into a XF^e96 Seahorse Flux Analyzer. Normalization of values to cell number was done using a CyQuant assay (Thermo). Data analysis was performed using Wave (Agilent) and GraphPad Prism.

Extracellular Lactate Measurement: Extracellular lactate measurement was performed using a YSI STAT 2300 Lactate analyzer. Buffer and calibrant solutions were prepared per manufacturer directions. A fresh lactate membrane was inserted and allowed to calibrate for 24 h. Stable resting lactate membrane currents were ensured prior to measurements. D35s dishes were plated with N- and SuHx-MVEC with and without MQ or HC treatment (24 h).At 24 h, media supernatant was extracted and cells were tryspinized and counted (Scepter cell counter, Millipore). The supernatant samples were stored at -80ºC. Samples were run in batches with untreated and treated normoxic and SuHx samples run sequentially. The results were normalized for cell count and to the normoxic control.

Targeted Metabolomics: N- and SuHx-MVECs were washed three times with ice-cold phosphate buffered saline (PBS). Samples were lysed using ice-cold 80% HPLC-grade methanol (Fisher Scientific) diluted with 20% mass-spec (MS)-grade water. Samples were centrifuged (and cell pellets saved for total protein quantification) and the supernatant was stored overnight at -80°C, then evaporated using a speed vacuum followed by lyophilization. The dried metabolites were resuspended in 50% (vol/vol) acetonitrile diluted with MS-grade water. An Agilent 1260 HPLC and 6490 triple-quadrupole (QQQ) mass spectrometer were used to assess the metabolites associated with glycolysis, the TCA cycle, and energetics. Full details of the LC/MS parameters are provided in Supplementary Table 2. TableAgilent MassHunter and Agilent Qualitative and Quantitative Analysis Software packages were used to assess and quantify the metabolic profiles of the

samples. In order to identify the relevant glycolytic, TCA cycle, and energetic compounds, pure standards were assessed under the same conditions as the samples in order to determine the optimal precursor/product ion transitions, collision energies, and ion polarity for each metabolite. Metabolite peaks were integrated for raw intensities. The total protein concentration of each sample was determined via a FilterMax F5 microplate reader and a Bovine Serum Albumin (BSA) standard. This total protein concentration was then used to normalize the raw intensities determined for each of the samples.

Intracellular Ca^{2+} measurements: Cells were seeded on glass coverslips (50-60% confluence; 24 h incubation in DMEM 5% FBS media) and loaded with Fura-2AM (5 μM; 1 h)before being placed in a temperature-controlled flow chamber as described previously (53). The perfusate used was a modified Krebs buffer containing (in mM): 118 NaCl, 4.7 KCl, 0.57 $MgSO_4$, 1.18 KH_2PO_4, 25 $NaHCO_3$, 2.5 $CaCl_2$ and 10 glucose gassed with 16% O_2 and 5% CO_2. After establishment of stable baseline, F_{380}/F_{380} was recorded (Incytim2 software). $[Ca^{2+}]_i$ was estimated from F_{340}/F_{380} measured in calibration solutions with Ca^{2+} concentrations of 0–1350 nM (Molecular Probes, Eugene, OR).

Intracellular ROS measurements: MVEC were infected with a roGFP-GRX1 plasmid delivered in a baculovirus vector (Premo ROS sensor, Life biotechnologies) at 80 MOI. At 48 h, cells were imaged and the F_{400}/F_{490} was calculated as described previously (53).

Data Analysis/Statistics: All values are expressed as means ± SE. For roGFP measurements, data were collected from up to 30 cells and the values were averaged to obtain a single value for each experiment. All experiments were performed using cells isolated from at least 5 different rats. Cells from different animals were not pooled during isolation, so each “n” represents cells isolated exclusively from one animal. For SeaHorse experiments, technical replicates from 4-6 wells were averaged to yield one value per animal. Similarly, mitochondrial length distribution data from multiple microscopy images using cells isolated from the same animal were averaged to yield a single biologic “n”. Data were compared using unpaired Student’s *t*-test, Mann-Whitney U/Kruskal-Wallis tests for non-parametric data, or two-way ANOVA (with post-hoc Tukey’s test) to determine the effect of treatment across multiple groups.

The earthmover distance (EMD) metric was used to compare differences between the length/number distributions between N- and SuHx-MVEC mitochondria. This statistic can be used to evaluate changes in the distribution of non-parametric histogram data(40, 41). EMD was calculated using the Momito program written by Ouellet et al (41). As described previously(41), the difference between two length distribution curves was considered significant if the EMD between the two groups was significantly higher than the intra-group differences in EMD within each individual group (compared using ANOVA, with Holm-Sidak post-hoc). A *P* value < 0.05 was accepted as statistically significant for all experiments.

Results

Following induction of experimental PAH, SuHx rats exhibited significant increases in RVSP, RV/LV+S and RV/body weight at the end of 5 weeks (Figure 1A-D). N- and SuHx-MVECs obtained from these animals were used for all subsequent studies. Similar to previous results in confocal images of Mito-RFP tagged MVECs (53), fragmentation was significantly increased in MitoTracker labeled SuHx-MVEC mitochondria (Figure 1E-F). We previously showed that application of MQ acutely normalized total ROS levels in SuHx-MVEC (53). To determine whether mtROS contributes to mitochondrial fragmentation, we imaged N- and SuHx-MVECs following MQ treatment. As shown in Figure 2A, MQ treatment had no effect on mitochondrial fragmentation in N-MVEC; however, MQ significantly attenuated fragmentation (evidenced by a downward shift of the mitochondrial length-distribution curve) in SuHx-MVEC (Figure 2B,C).

We correlated these imaging findings with phosphorylation of dynamin related protein-1 (Drp1), a GTPase that is critical for initiation of mitochondrial fission (14, 67). Similar to prior reports in other cell types (37, 68, 72), we previously found that fragmentation in SuHx-MVECs was accompanied by increased pSer616Drp1 levels (53). MQ treatment had no effect on Drp1 levels (phosphorylated or total) in N-MVEC but attenuated Drp1 phosphorylation in SuHx-MVEC (Figure 2D-E).

To further determine whether increased mtROS could promote fragmentation in SuHx-MVEC, we performed a "gain-of-function" experiment where N-MVEC were treated with Antimycin A (AA), a drug that inhibits electron transport at Complex III and induces mtROS production (10, 27, 50). Increasing ROS levels with AA (10 μM; 20 minutes) treatment in N-MVEC was confirmed using the ratiometric redox sensor, roGFP (Figure 3A). To

determine whether AA-induced mtROS production caused fragmentation, we measured mitochondrial fragmentation in AA-treated N-MVECs. As shown in Figure 3B-C, mitochondrial fragmentation was significantly increased in AA-treated N-MVECs and was similar to values observed in untreated SuHx-MVECs. We previously observed that mtROS increases $[Ca^{2+}]_i$ by activating the TRPV4 channel (53). To determine whether AA-induced mtROS generation promoted fission via TRPV4, we measured the effect of AA on mitochondrial fragmentation in N-MVEC treated with a TRPV4 inhibitor (HC), and observed attenuation of AA-induced mitochondrial fragmentation (HC+AA).

Since impairment or loss of counter-regulatory fusion mechanisms may be sufficient to increase fission, we examined whether loss of fusing capacity was contributing to increased SuHx-MVEC mitochondrial fragmentation. To initiate fusion, we used brief serum starvation (2 hours incubation in DMEM without FBS), which has previously been shown to potently induce fusion (47). We observed significantly more elongated mitochondria in N-MVECs with serum starvation (Figure 4A-B). Serum starvation of SuHx-MVECs also significantly improved mitochondrial fragmentation (Figure 4C-D). As shown in Figure 4E-F, we also measured levels of Mitofusin-2 (Mfn-2), a critical regulator of mitochondrial fusion, and found no differences in Mfn-2 expression between N- and SuHx-MVECs. These data suggest that fusion mechanisms were intact and impairment of fusion was not contributing to mitochondrial fragmentation in SuHx-MVEC.

Our previous work showed that, in MVECs, both endogenous and exogenous ROS can activate TRPV4 to increase $[Ca^{2+}]_i$ and that quenching mtROS with MQ normalized $[Ca^{2+}]_i$ in SuHx-MVECs (53, 54, 56). Thus, we hypothesized that mtROS may promote mitochondrial fragmentation by activating TRPV4. First, we measured ROS levels when TRPV4 was inhibited to determine whether increased $[Ca^{2+}]_i$ itself can contribute to ROS formation in N- and SuHx-MVECs. As shown in Figure 5A, treatment with GSK22193875 (GSK2; 30 nM) a specific inhibitor of TRPV4 previously shown to decrease $[Ca^{2+}]_i$ in SuHx-MVECs (53), had no effect on ROS levels in SuHx-MVEC. These data are consistent with previous results obtained using HC-067047 (HC; 10 μM), a different TRPV4 inhibitor (53). Next, we measured fragmentation following treatment with both GSK2 and HC. As shown in Figure 5B-F, similar to MQ treatment, TRPV4 inhibition with either HC or GSK2 attenuated fragmentation in SuHx-MVECs.

Since we hypothesized that mtROS-induced Ca^{2+} influx via TRPV4 was responsible for mitochondrial fragmentation, we questioned whether TRPV4 activation alone would be sufficient to induce fragmentation in N-MVECs. Our previous work showed that total TRPV4 protein levels were similar in N- and SuHx-MVECs (53), but the effect of direct TRPV4 activation on $[Ca^{2+}]_i$ in N- and SuHx-MVECs was unknown. Thus, we measured $[Ca^{2+}]_i$ in N- and SuHx-MVECs following treatment with GSK1016790A (GSKA; 1.5 μM) a specific TRPV4 agonist. Surprisingly, $[Ca^{2+}]_i$ was not changed in N-MVECs following GSKA exposure (Figure 6A). In contrast, GSKA induced a large increase in $[Ca^{2+}]_i$ in SuHx-MVECs (Figure 6B), suggesting that although total TRPV4 protein expression was similar in N- and SuHx-MVECs, TRPV4 activation was enhanced in SuHx-MVECs. To confirm this finding and determine whether mtROS were involved, we measured GSKA-induced Ca^{2+} influx after MQ treatment. Similar to our prior report (53), treatment of SuHx-MVECs with MQ decreased basal $[Ca^{2+}]_i$ (Figure 6C). Interestingly, MQ treatment also attenuated the GSKA-induced increase in $[Ca^{2+}]_i$ in SuHx-MVECs (Figure 6C-D), suggesting that mtROS, in addition to directly activating TRPV4, might also contribute to sensitization of TRPV4 to chemical agonists.

Given our $[Ca^{2+}]_i$ data, we next hypothesized that TRPV4 agonism might worsen fragmentation in SuHx-MVECs. GSKA treatment did not significantly alter mitochondrial fragmentation in N-MVEC, likely due to the lack of effect on GSK on $[Ca^{2+}]_i$ in these cells. In SuHx-MVECs, GSKA treatment increased the percentage of shorter mitochondria, but this small shift in the length/number distribution was not statistically significant (Supplemental S2).

Lastly, since TRPV4 blockade and mtROS quenching similarly improved mitochondrial fragmentation, we questioned whether these changes in mitochondrial fragmentation were accompanied by improvement in mitochondrial respiration. Consistent with our previously reported data (53), basal OCR was decreased while extracellular acidification rate (ECAR) was increased in SuHx-MVEC (Figure 8). Despite improving mitochondrial fragmentation and $[Ca^{2+}]_i$, 1 h treatment with MQ or HC did not reverse changes in SuHx-MVEC OCR and ECAR (data not shown). Hypothesizing that changes to mitochondrial respiration following ROS quenching might occur later than changes to mitochondrial fragmentation, we measured OCR and ECAR after 24 h MQ or HC treatment. We encountered significant batch variation in the raw values of OCR and ECAR across animals; thus, we normalized values to untreated normoxic controls, but have presented the raw values

in the traces shown in Figure 7A-D and in Supplementary Table 1. As shown in Figure 7, 24 h MQ treatment improved OCR and ECAR in SuHx-MVECs. Interestingly, HC treatment decreased ECAR, but not OCR, in SuHx-MVECs.

While the ECAR results, combined with the decreased basal/maximum OCR, were suggestive of glycolytic shift, we sought to confirm these observations using additional measurements of glycolysis at baseline and with drug treatment. Targeted metabolomics analysis of key glycolysis metabolites in N- and SuHx-MVECs revealed upregulation of glycolysis metabolites as well as increased ATP (Figure 8A-C). In addition to increased levels of intracellular lactate, as shown in Figure 8D, extracellular lactate levels were increased at baseline in SuHx-MVECs, but were reduced with MQ and HC (24 h) treatment (Figure 8D).

Discussion

In this study, we show that MVECs isolated from a rodent model of PAH exhibit significant mitochondrial fragmentation that can be modulated by mtROS-induced Ca^{2+} influx via the TRPV4 channel. Furthermore, our data suggest that quenching mtROS attenuates both morphological and functional abnormalities in SuHx-MVECs. Mitochondrial dysfunction has been implicated in the pathobiology of many diseases, including PAH (49). For instance, decreasing fission by either genetic silencing of Drp1 or use of the Drp1 inhibitor P110 attenuated pulmonary artery smooth muscle cell proliferation (37) and RV dysfunction (64) in animal models of PAH, suggesting that restoring mitochondrial morphology to a more networked state is sufficient to ameliorate cellular dysfunction. Unlike PASMCs, less is known about the mechanisms regulating mitochondrial fission/fusion in MVECs during PAH. This point is relevant because MVECs are a component of plexiform lesions (30), a key feature of PAH (36), and we, along with several other groups, recently reported significant endothelial dysfunction, including EndMT, in multiple PAH models (35, 57, 60). Work in a variety of cell types, including MVECs, epithelial and cancer cells, suggests that the underpinnings of EndMT may be metabolic in origin, as induction of EndMT is typically accompanied by significant metabolic reprogramming (26, 73). Our current work also suggests an association between altered mitochondrial energetics and mitochondrial fragmentation in SuHx-MVECs, with mitochondrial structure being modified by inhibiting Ca^{2+} entry or quenching mtROS (53). While similar manipulations also normalize SuHx-MVEC migration and

proliferation(53), it remains be seen whether improvement in mitochondrial fragmentation alone is sufficient to reverse abnormal PAH EC cell function. Further experiments measuring migration and proliferation in SuHx-MVECs using fusion-inducing agents will be needed to distinguish whether the effects of inhibiting mtROS-induced Ca^{2+} entry on migration and proliferation are due to improvement of mitochondrial structure or whether mitochondrial fragmentation is a simply marker in cells with high $[Ca^{2+}]_i$.

A link between Ca^{2+} homeostasis and mitochondrial structure/function has long been appreciated. Mitochondria act as a local sink for rising Ca^{2+}, but increasing $[Ca^{2+}]_i$ also alters mitochondrial function and morphology (31, 58). We show that inhibition of TRPV4 in SuHx-MVECs attenuates baseline $[Ca^{2+}]_i$ and fission to an extent similar to quenching mtROS. That TRPV4 activation is downstream of mtROS suggests that ROS-induced Ca^{2+} influx via TRPV4 contributes to increased fission in SuHx-MVECs. Since we observed similar attenuation of mitochondrial fragmentation using two different inhibitors of TRPV4 previously shown to be specific for this channel (63, 71), it is unlikely that the observed effect of TRPV4 inhibition on mitochondrial fragmentation is due to nonspecific blockade of other Ca^{2+} channels. However, a contribution to increased basal $[Ca^{2+}]_i$ in SuHx-MVECs via increased ER release and/or decreased mitochondrial Ca^{2+} uptake mechanisms cannot be definitively excluded based on the current studies. With regards to the pharmacokinetics of TRPV4 inhibition, we previously showed that perfusing SuHx-MVECs with either HC or GSK2 decreased basal $[Ca^{2+}]_i$ levels within a few minutes (53); thus, in our current mitochondrial morphology studies, we initially used a short incubation time (1 h) to study the effect of TRPV4 inhibition on mitochondrial fragmentation. TRPV4 has been previously implicated in various models of lung injury and in regulating hypoxic pulmonary vasoconstriction (4, 9, 24, 25) and recent evidence from the cerebral vasculature suggests that mtROS may activate TRPV4 to promote brain EC dysfunction after traumatic brain injury (59). However, a role for this channel in regulating mitochondrial fragmentation has, to our knowledge, not been previously described.

The mechanism by which increased $[Ca^{2+}]_i$ induces mitochondrial fission is not fully understood; however, emerging evidence in neurons suggests that activation of plasma membrane channels leads to Ca^{2+}-dependent phosphorylation of Drp1, which in turn promotes fission (13, 28). In this study, we quantified mitochondrial network architecture using a newer, unsupervised algorithm to better understand the relationship

between $[Ca^{2+}]_i$ and mitochondrial structure in SuHx-MVECs. To assure image quality of mitochondrial networks, we obtained mitochondrial images on live, sub-confluent MVEC monolayers imaged in a temperature-controlled, gassed chamber, to minimize cellular stresses that may occur with specimen processing and can impact mitochondrial morphology/dynamics. Additionally, we corroborated changes in mitochondrial fission with corresponding increase or decrease in levels of phosphorylated Drp1. Specifically, differences in mitochondrial fragmentation between N-MVECs, SuHx-MVECs and MQ-treated SuHx-MVECs correlated with corresponding changes in phosphorylation of Drp1 at the Ser616 residue, which is critical for Drp1 recruitment to the mitochondria. In addition to Ser616, the 637 serine residue of Drp1 also plays a role in regulating Drp1 activity. The role of Ser637 phosphorylation in Drp1 recruitment to mitochondria in ECs in MVECs remains under investigation. We previously reported that phosphorylation of Ser637 was increased in SuHx-MVECs (53). This finding was in contrast to the role of Ser637 in regulating fission in HeLa cells, where de-phosphorylation of Ser637 by calcineurin has been shown to be important for initiation of fission (13). Of note, the opposite (i.e. increased Ser637 phosphorylation associated with fission) has been shown in kidney ECs (68). To determine whether changes in Ser637 phosphorylation were contributing to increased fission in SuHx-MVECs, we treated SuHx-MVECs with cyclosporine A, a calcineurin inhibitor, reasoning that if dephosphorylation of Ser637 by calcineurin was contributing to increased fission, inhibiting this pathway would improve fragmentation in SuHx-MVECs. However, we did not observe any change in SuHx-MVEC fragmentation (Supplemental Figure S3). These data, along with our previous data showing increased Ser637 phosphorylation of Drp1 in SuHx-MVECs at baseline (53), suggest that de-phosphorylation of Ser637 does not appear to be playing a major role in promoting increased fission in SuHx-MVECs.

Other proteins involved in mitochondrial machinery, including the Rho-GTPase Miro1, which regulates mitochondrial movement on microtubules, are also regulated by $[Ca^{2+}]_i$ (8). Furthermore, Drp1 is one part of a complex of proteins, such as mitochondrial fission factor (Mff) (21), and mitochondrial dynamics protein 49/51 (MiD49/51) (42), that are required for successful execution of fission. Further work is needed to determine which, if any, of the other components of the fission machinery are also abnormal in SuHx-MVECs.

Our serum starvation data suggest that induction of fusion via alternative pathways is able to partially overcome increased mitochondrial fragmentation in SuHx-MVECs. Furthermore, levels of the critical fusion

regulator Mfn-2 do not appear to be significantly different in SuHx-MVECs. These data suggest that the primary deficit in mitochondrial structure in SuHx-MVECs is increased fission rather than inability to fuse. However, more work using alternative fusion-inducing stimuli and/or overexpression of proteins involved in fusion is needed to conclusively determine the role of fusion in SuHx-MVECs. Importantly, fission/fusion dynamics exist within the larger context of biogenesis (i.e. generation of new mitochondria) and mitophagy (i.e. disposal of severely dysfunction mitochondria). Thus, while fission is clearly increased and fusion does not appear to be impaired in SuHx-MVECs, more studies are needed to determine if additional deficits in initiation of mitophagy and/or biogenesis are contributing to the continued presence of fragmented dysfunctional mitochondria in SuHx-MVECs.

Similar to increased $[Ca^{2+}]_i$, significant evidence points to the role of increased ROS in promoting mitochondrial fission (22, 32, 66, 78). Our data suggest a link between these two regulators of mitochondrial fragmentation; that is, the effects of ROS on mitochondrial fragmentation may be regulated via ROS-induced increases in $[Ca^{2+}]_i$ via TRPV4. That inhibiting mtROS decreased, and increasing mtROS enhanced, fragmentation, while MQ treatment had no effect in N-MVECs, suggests that the effect of MQ on mitochondrial fragmentation is unlikely to be due to non-targeted effects of this drug. The dose of MQ used has previously been shown to effectively quench ROS production at Complex III (10). Although we show Complex III ROS generation (i.e., AA treatment) was sufficient to cause fragmentation, it is possible at mtROS generation at other complexes may also produce similar fragmentation and changes in $[Ca^{2+}]_i$. Further, we used short time points (1 h) in our MQ treatment experiments since we previously observed that MQ decreases basal $[Ca^{2+}]_i$ acutely in SuHx-MVECs. However, we did not perform time course experiments with MQ; thus, it is possible that improvement in mitochondrial structure may occur even earlier than our studied time point.

Our data suggest that mtROS might increase the sensitivity of TRPV4 to GSKA, since agonist-induced Ca^{2+} influx was greater in untreated SuHx-MVECs, which have higher mtROS levels at baseline. Moreover, quenching mtROS attenuated the GSKA response in SuHx-MVECs. The lack of GSKA-induced Ca^{2+} influx in N-MVECs provides an explanation for why mitochondrial fragmentation did not significantly change in GSKA-treated N-MVECs. Interestingly, although GSKA induced a significant Ca^{2+} influx in SuHx-MVECs, additional fragmentation was not observed, possibly because the mitochondrial network was already extensively

fragmented at baseline, and further fission was not possible. Another possibility is that the transient GSKA-induced Ca^{2+} spike in MVECs (1) may not be long enough to induce fission. In neurons, for instance, a sustained $[Ca^{2+}]_i$ elevation is needed for induction of fission (31). . With regards to increased GSKA sensitivity in SuHx-MVECs at baseline, and MQ treatment attenuating this response, we hypothesize that this may be due to regulation of TRPV4 translocation. Recent evidence in macrophages suggests that TRPV4 translocates to the cell surface in response to injurious stimuli (51). Caveolin-1 (Cav-1) is a key protein that regulates membrane trafficking of proteins, including Ca^{2+} channels, into the cell membrane. Regulated in part by redox-sensitive tyrosine phosphorylation (15), Cav-1 was recently shown to compartmentalize (and immunoprecipitate) with TRPV4 (23); thus, we hypothesize that the mechanism behind our observed findings may involve trafficking of TRPV4 to the membrane by ROS-induced activation of Cav-1. Of note, however, we (54) and others (69, 74) have previously shown that TRPV4 activity can also be modulated by phosphorylation. Thus, another possible explanation for our GSKA-induced Ca^{2+} influx data is that mtROS may directly oxidize intermediary kinases that then regulate the sensitivity to TRPV4 to activating stimuli by phosphorylating this channel. Further experiments such as membrane fractionation to look for changes in TRPV4 protein, phospho-tyrosine co-immunoprecipitation or measurement of GSKA-induced Ca^{2+} influx following inhibition of Cav-1 and/or kinases known to phosphorylate TRPV4 are needed to further dissect the mechanisms by which ROS activate TRPV4 in SuHx-MVECs.

While both inhibition of mtROS and reduction of $[Ca^{2+}]_i$ improved mitochondrial fragmentation, only MQ improved mitochondrial function (i.e. respiration). Even after ensuring cell viability and number before and after our respiration measurements, baseline respiration values for SuHx-MVECs were low, especially in comparison to other cell types. Interestingly, HC did not improve mitochondrial respiration in SuHx-MVECs. One possibility is that while Ca^{2+} dependent mechanisms regulate mitochondrial movement, in the presence of ongoing increased mtROS generation improving fission by inhibiting Ca^{2+} entry may be insufficient to rescue the metabolic abnormalities in SuHx-MVEC, and would simply lead to re-fragmentation at a later time point as ROS levels continue to rise. Another possibility is that mtROS may be affecting mitochondrial signaling pathways related to respiration independent of $[Ca^{2+}]_i$, in which case decreasing $[Ca^{2+}]_i$ alone may be insufficient to reverse mtROS-induced decreases in oxidative phosphorylation, especially since we showed

that TRPV4 inhibition decreases $[Ca^{2+}]_i$ but not mtROS, in SuHx-MVECs. Interestingly, despite not improving mitochondrial respiration, TRPV4 inhibition significantly improved ECAR, suggesting that TRPV4-mediated Ca^{2+} entry may also regulating glycolysis directly, independent of mitochondrial fission. While our ECAR data, taken together with our metabolomic and extracellular lactate data implicate shifts in glycolysis, additional experiments aimed at specifically interrogating glycolytic flux in SuHx-MVECs are needed.

Together, our respiration and roGFP data suggest that mtROS generation is upstream of increased $[Ca^{2+}]_i$ in SuHx-MVECs. However, whether mtROS production in SuHx-MVECs is triggered by underlying shifts in cell metabolism is unclear. For instance, evidence in cancer and immune cells suggests that, in the presence of glycolytic shift, increased dependence on glutamine as a source for TCA intermediates may fuel ROS production (34, 70). On the other hand, Diebold et al (17) showed that in lung ECs, mtROS production at complex III was sufficient to decrease basal respiration (similar to our current findings) and induce metabolic dysfunction. As mentioned earlier, restoration of mitochondrial fusion/fission dynamics towards a more fused state was sufficient to ameliorate cardiac dysfunction in PAH and other models of injury (37, 64). However, if the underlying metabolic dysfunction is not corrected, inhibiting pathways such as mtROS, $[Ca^{2+}]_i$ or even Drp1 may provide short-term restoration of cellular function, but mitochondrial dysfunction may return as the inhibitors of these downstream pathways are degraded or exported out of the cell. Thus, further work is needed to more mechanistically understand the driving forces behind the ROS and Ca^{2+}-mediated dysfunction in mitochondrial dynamics and metabolism described herein.

In summary, our current study suggests an interplay between mtROS, $[Ca^{2+}]_i$ and mitochondrial fragmentation and function in MVECs in PAH (Figure 9). Our data suggests that this process may be self-propagating, with increased production of mtROS inducing Ca^{2+} influx via TRPV4, which in turn promotes mitochondrial fission and mtROS production. On the other hand, while inhibition of TRPV4 improves mitochondrial fragmentation without any effects on respiration, inhibiting mtROS restores both mitochondrial fragmentation and respiration in SuHx-MVECs, suggesting that mtROS production may be fueled by additional, possibly metabolic, factors. Additional studies aimed at understanding the metabolic underpinnings of mtROS production in SuHx-MVECs will be informative in further elucidating the mechanisms of microvascular endothelial dysfunction in PAH.

Nonetheless, given the beneficial effects of reducing mtROS in mitochondrial and cellular function, specifically targeting mtROS in MVECs may be an attractive candidate for treating PAH.

Acknowledgments: We thank Drs. Jimmie Sylvester and David Pearse for their thoughtful comments and guidance on experimental design and data analysis. We also thank Dr. Michael Caterina for providing expertise regarding TRPV4 and the Johns Hopkins School of Medicine (JHUSOM) Microscope Facility for assistance with fluorescence confocal imaging.

Funding Support for this study was provided by the National Heart, Lung and Blood Institute Grants F32HL124930 and K08HL132055 (KS), R01HL073859, R25HL084762 and R01HL126514 (LAS), F32HL124727 and K08HL133475 (JH) and T32HL007534 (KS and JH). Additional support includes a Gilead PAH Research Scholar Award and Parker B. Francis Research Opportunity Award (KS), as well as NIH S10OD016374 (S. Kuo, JHUSOM Microscope facility)

Author Contributions: Conception and design of experiments (KS, LS, HY, ZB, BK, AL, JZ,JH, CK, MA) , acquisition, analysis or interpretation of data and drafting/critical review of manuscript (KS, LS, JH, BK, AL, CK, MA, SC, MD, LS). All authors approved the final version of the manuscript.

Figure Legends

Figure 1. Hemodynamics and microvascular endothelial cell (MVEC) mitochondrial fragmentation in the SuHx model of PAH. **A)** Representative tracings of closed-chest right ventricular systolic pressure (RVSP) measurement in Normoxic and SuHx rats. Scatter plots showing mean±SEM for **B)** RVSP, **C)** right ventricle/left ventricle+septal weight (RV/LV+S) and **D)** RV/body weight in Normoxic (N) and SuHx rats. * denotes significant difference from normoxic animals (t-test). **E)** Representative photomicrographs and reconstructed mitochondrial network images for N- and SuHx-MVECs. **F)** Length distribution curves for N- and SuHx-MVEC mitochondria. * denotes significant difference from N-MVECs (ANOVA), n=5 per group

Figure 2. Effect of mtROS quenching on mitochondrial fragmentation. **A)** Representative mitochondrial network images in N- and SuHx-MVECs in the absence and presence of MitoQ (MQ; 1μM – 1 hour). **B-C)**

Length distribution curves (with SE at each distribution length) for mitochondria from N- and SuHx-MVECs with and without MQ treatment. n= 5 per group (ANOVA). **D)** Western blot and **E)** densitometry showing pSer616Drp1 and total Drp1 protein levels in N- and SuHx-MVECs with and without MQ treatment, each n from a different animal. * denotes significant difference from normoxic control, ** denotes significant difference from SuHx-MVECs (ANOVA).

Figure 3. mtROS production in N-MVECs. **A)** Scatter plot showing mean±SEM for roGFP ratios in N-MVECs with and without treatment with Antimycin A (AA; 10 μM). **B)** Representative mitochondrial network images in untreated, AA-treated and HC+AA treated N-MVEC **C)** Length distribution curves for N-MVEC mitochondria in untreated, AA-treated and HC+AA treated N-MVECs. * denotes significant difference from normoxic control (ANOVA), n=5 per group.

Figure 4. Induction of fusion in N- and SuHx-MVEC. Representative images (**A, C)** and length distribution curves **(B, D)** in N- and SuHx-MVEC in basal (5% FBS) serum and after incubation in serum-free media for 2 hours.* denotes significant difference from untreated SuHx control. N=10-15 images from 5 different animals. **E)** Representative immunoblots **(F)** and densitometry **(G)** showing Mitofusin-2 protein levels in N- and SuHx-MVECs. * denotes significant difference from N-MVEC control; ** denotes significant difference from SuHx control (ANOVA). n=5 per group

Figure 5. TRPV4 and mitochondrial fragmentation in SuHx-MVECs. **A)** Scatter plot showing mean±SEM for roGFP ratios in N- and SuHx-MVECs with and without treatment with GSK2193874 (GSK2; 30 nM). n=5-6 (from different animals) per group. **B)** Representative network images and **C-F)** length distribution curves for N- and SuHx-MVEC mitochondria with and without treatment with two TRPV4 inhibitors: HC-067047 (HC; 10 μM) and GSK2 (30 nM) * denotes significant difference from SuHx-MVECs (ANOVA)

Figure 6. GSKA-induced Ca^{2+} influx in SuHx-MVECs. **A-B)** Representative traces showing $[Ca^{2+}]_i$ in N- and SuHx-MVECs with and without MQ treatment at baseline and following perfusion with TRPV4 agonist GSK1016790A (GSKA; 1.5 μM).**C)** Scatter plot showing mean±SEM baseline and GSKA-induced changes in $[Ca^{2+}]_i$ in N- and SuHx-MVECs in the absence and presence of MQ. **D)** Scatter plot showing mean±SEM change in $[Ca^{2+}]_i$ (nM) in N-MVEC before and after GSKA (N vs. N+GSKA), untreated SuHx-MVEC before and

after GSKA (S vs. S+GSKA) and MQ-treated SuHx-MVEC before and after GSKA (S+MQ vs. S+MQ+GSKA). * denotes significant difference from N-MVECs. ** denotes significant difference from SuHx-MVECs (ANOVA).

Figure 7. Effect of mtROS and Ca^{2+} inhibition on mitochondrial respiration. Curves of mitochondrial oxygen consumption rate (OCR) in N- and SuHx-MVECs at baseline and following treatment with **A-B)** MQ and **C-D)** HC. Scatter plots showing mean±SEM for **D)** basal OCR and **E)** ECAR in N-MVECs normalized to untreated N-MVEC controls. * denotes significant difference from N-MVEC control; ** denotes significant difference from SuHx-MVECs. (ANOVA)

Figure 8. A) Heatmap showing fold change differences in glycolysis and TCA metabolites in N- and SuHx-MVECs (n=cells isolated from 8 individual animals). B) Table showing median fold change (and IQR) for metabolite levels. n=8 biological replicates. C) Scatter plot showing fold change in ATP levels in SuHx-MVECs. D) Scatter plot showing fold change in extracellular lactate at baseline and following treatment (24h) with MitoQ (MQ) or HC-067047 (HC). * denotes significant difference from normoxic control (t-test); ** denotes significant difference from untreated SuHx-MVEC control (ANOVA).

Figure 9. Schematic describing our proposed pathway of interaction between TRPV4 and mitochondrial fragmentation in SuHx-MVECs (solid lines) as well as other established pathways linking mitochondrial dysfunction to EC migration/proliferation (dashed lines). [a] Increased ROS production, decreased basal / maximal respiration, increased fission, evidence of glycolytic shift. [b] Direct effects of mtROS on transcription(3) [c] Changes in fuel utilization following glycolytic shift providing carbons (i.e. anaplerosis) for generation of metabolites essential for biosynthetic activities such as proliferation(79).

References

1. **Adapala RK, Talasila PK, Bratz IN, Zhang DX, Suzuki M, Meszaros JG, and Thodeti CK**. PKCα mediates acetylcholine-induced activation of TRPV4-dependent calcium influx in endothelial cells. *Am J Physiol Heart Circ Physiol* 301: H757-765, 2011.
2. **Aggarwal S, Gross CM, Sharma S, Fineman JR, and Black SM**. Reactive oxygen species in pulmonary vascular remodeling. *Compr Physiol* 3: 1011-1034, 2013.
3. **Al-Mehdi AB, Pastukh VM, Swiger BM, Reed DJ, Patel MR, Bardwell GC, Pastukh VV, Alexeyev MF, and Gillespie MN**. Perinuclear mitochondrial clustering creates an oxidant-rich nuclear domain required for hypoxia-induced transcription. *Science signaling* 5: ra47, 2012.

4. **Alvarez DF, King JA, Weber D, Addison E, Liedtke W, and Townsley MI**. Transient receptor potential vanilloid 4-mediated disruption of the alveolar septal barrier: a novel mechanism of acute lung injury. *Circulation research*\ 99\: 988\, 2006.
5. **Archer SL**. Mitochondrial Dynamics — Mitochondrial Fission and Fusion in Human Diseases. *New England Journal of Medicine* 369: 2236-2251, 2013.
6. **Archer SL, Gomberg-Maitland M, Maitland ML, Rich S, Garcia JG, and Weir EK**. Mitochondrial metabolism, redox signaling, and fusion: a mitochondria-ROS-HIF-1alpha-Kv1.5 O2-sensing pathway at the intersection of pulmonary hypertension and cancer. *Am J Physiol Heart Circ Physiol* 294: H570-578, 2008.
7. **Archer SL, Huang J, Henry T, Peterson D, and Weir EK**. A redox-based O2 sensor in rat pulmonary vasculature. *Circ Res* 73: 1100-1112, 1993.
8. **Bagur R, and Hajnóczky G**. Intracellular Ca2+ Sensing: Its Role in Calcium Homeostasis and Signaling. *Molecular cell* 66: 780-788, 2017.
9. **Balakrishna S, Song W, Achanta S, Doran SF, Liu B, Kaelberer MM, Yu Z, Sui A, Cheung M, Leishman E, Eidam HS, Ye G, Willette RN, Thorneloe KS, Bradshaw HB, Matalon S, and Jordt SE**. TRPV4 inhibition counteracts edema and inflammation and improves pulmonary function and oxygen saturation in chemically induced acute lung injury. *Am J Physiol Lung Cell Mol Physiol* 307: L158-172, 2014.
10. **Bell EL, Klimova TA, Eisenbart J, Moraes CT, Murphy MP, Budinger GR, and Chandel NS**. The Qo site of the mitochondrial complex III is required for the transduction of hypoxic signaling via reactive oxygen species production. *The Journal of cell biology* 177: 1029-1036, 2007.
11. **Bonnet S, Michelakis ED, Porter CJ, Andrade-Navarro MA, Thebaud B, Bonnet S, Haromy A, Harry G, Moudgil R, McMurtry MS, Weir EK, and Archer SL**. An abnormal mitochondrial-hypoxia inducible factor-1alpha-Kv channel pathway disrupts oxygen sensing and triggers pulmonary arterial hypertension in fawn hooded rats: similarities to human pulmonary arterial hypertension. *Circulation* 113: 2630-2641, 2006.
12. **Bowers R, Cool C, Murphy RC, Tuder RM, Hopken MW, Flores SC, and Voelkel NF**. Oxidative stress in severe pulmonary hypertension. *Am J Respir Crit Care Med* 169: 764-769, 2004.
13. **Cereghetti GM, Stangherlin A, Martins de Brito O, Chang CR, Blackstone C, Bernardi P, and Scorrano L**. Dephosphorylation by calcineurin regulates translocation of Drp1 to mitochondria. *Proceedings of the National Academy of Sciences of the United States of America* 105: 15803-15808, 2008.
14. **Cho B, Choi SY, Cho HM, Kim HJ, and Sun W**. Physiological and pathological significance of dynamin-related protein 1 (drp1)-dependent mitochondrial fission in the nervous system. *Experimental neurobiology* 22: 149-157, 2013.
15. **Coelho-Santos V, Socodato R, Portugal C, Leitao RA, Rito M, Barbosa M, Couraud PO, Romero IA, Weksler B, Minshall RD, Fontes-Ribeiro C, Summavielle T, Relvas JB, and Silva AP**. Methylphenidate-triggered ROS generation promotes caveolae-mediated transcytosis via Rac1 signaling and c-Src-dependent caveolin-1 phosphorylation in human brain endothelial cells. *Cellular and molecular life sciences : CMLS* 73: 4701-4716, 2016.
16. **Contreras L, Drago I, Zampese E, and Pozzan T**. Mitochondria: the calcium connection. *Biochimica et biophysica acta* 1797: 607-618, 2010.
17. **Diebold LP, Gil HJ, Gao P, Martinez CA, Weinberg SE, and Chandel NS**. Mitochondrial complex III is necessary for endothelial cell proliferation during angiogenesis. *Nature Metabolism* 1: 158-171, 2019.
18. **Duong HT, Comhair SA, Aldred MA, Mavrakis L, Savasky BM, Erzurum SC, and Asosingh K**. Pulmonary artery endothelium resident endothelial colony-forming cells in pulmonary arterial hypertension. *Pulm Circ* 1: 475-486, 2011.
19. **Evrard SM, Lecce L, Michelis KC, Nomura-Kitabayashi A, Pandey G, Purushothaman KR, d'Escamard V, Li JR, Hadri L, Fujitani K, Moreno PR, Benard L, Rimmele P, Cohain A, Mecham B, Randolph GJ, Nabel EG, Hajjar R, Fuster V, Boehm M, and Kovacic JC**. Endothelial to mesenchymal transition is common in atherosclerotic lesions and is associated with plaque instability. *Nature communications* 7: 11853, 2016.
20. **Fiorio Pla A, Ong HL, Cheng KT, Brossa A, Bussolati B, Lockwich T, Paria B, Munaron L, and Ambudkar IS**. TRPV4 mediates tumor-derived endothelial cell migration via arachidonic acid-activated actin remodeling. *Oncogene* 31: 200-212, 2012.
21. **Gandre-Babbe S, and van der Bliek AM**. The novel tail-anchored membrane protein Mff controls mitochondrial and peroxisomal fission in mammalian cells. *Mol Biol Cell* 19: 2402-2412, 2008.
22. **Giedt RJ, Yang C, Zweier JL, Matzavinos A, and Alevriadou BR**. Mitochondrial fission in endothelial cells after simulated ischemia/reperfusion: role of nitric oxide and reactive oxygen species. *Free Radic Biol Med* 52: 348-356, 2012.

23. **Goedicke-Fritz S, Kaistha A, Kacik M, Markert S, Hofmeister A, Busch C, Banfer S, Jacob R, Grgic I, and Hoyer J**. Evidence for functional and dynamic microcompartmentation of Cav-1/TRPV4/K(Ca) in caveolae of endothelial cells. *European journal of cell biology* 94: 391-400, 2015.
24. **Goldenberg NM, Ravindran K, and Kuebler WM**. TRPV4: physiological role and therapeutic potential in respiratory diseases. *Naunyn-Schmiedeberg's archives of pharmacology* 2014.
25. **Goldenberg NM, Wang L, Ranke H, Liedtke W, Tabuchi A, and Kuebler WM**. TRPV4 Is Required for Hypoxic Pulmonary Vasoconstriction. *Anesthesiology* 122: 1338-1348, 2015.
26. **Guerra F, Guaragnella N, Arbini AA, Bucci C, Giannattasio S, and Moro L**. Mitochondrial Dysfunction: A Novel Potential Driver of Epithelial-to-Mesenchymal Transition in Cancer. *Frontiers in Oncology* 7: 295, 2017.
27. **Gusarova GA, Trejo HE, Dada LA, Briva A, Welch LC, Hamanaka RB, Mutlu GM, Chandel NS, Prakriya M, and Sznajder JI**. Hypoxia leads to Na,K-ATPase downregulation via Ca(2+) release-activated Ca(2+) channels and AMPK activation. *Mol Cell Biol* 31: 3546-3556, 2011.
28. **Han XJ, Lu YF, Li SA, Kaitsuka T, Sato Y, Tomizawa K, Nairn AC, Takei K, Matsui H, and Matsushita M**. CaM kinase I alpha-induced phosphorylation of Drp1 regulates mitochondrial morphology. *The Journal of cell biology* 182: 573-585, 2008.
29. **Huetsch JC, Jiang H, Larrain C, and Shimoda LA**. The Na+/H+ exchanger contributes to increased smooth muscle proliferation and migration in a rat model of pulmonary arterial hypertension. *Physiological reports* 4: 2016.
30. **Humbert M, Montani D, Perros F, Dorfmüller P, Adnot S, and Eddahibi S**. Endothelial cell dysfunction and cross talk between endothelium and smooth muscle cells in pulmonary arterial hypertension. *Vascul Pharmacol* 49: 113-118, 2008.
31. **Jeyaraju DV, Cisbani G, and Pellegrini L**. Calcium regulation of mitochondria motility and morphology. *Biochimica et Biophysica Acta (BBA) - Bioenergetics* 1787: 1363-1373, 2009.
32. **Jezek J, Cooper KF, and Strich R**. Reactive Oxygen Species and Mitochondrial Dynamics: The Yin and Yang of Mitochondrial Dysfunction and Cancer Progression. *Antioxidants (Basel, Switzerland)* 7: 2018.
33. **Lanna A, and Dustin ML**. Mitochondrial fusion fuels T cell memory. *Cell Research* 26: 969-970, 2016.
34. **Le A, Lane AN, Hamaker M, Bose S, Gouw A, Barbi J, Tsukamoto T, Rojas CJ, Slusher BS, Zhang H, Zimmerman LJ, Liebler DC, Slebos RJ, Lorkiewicz PK, Higashi RM, Fan TW, and Dang CV**. Glucose-independent glutamine metabolism via TCA cycling for proliferation and survival in B cells. *Cell metabolism* 15: 110-121, 2012.
35. **Mammoto T, Muyleart M, Konduri GG, and Mammoto A**. Twist1 in Hypoxia-induced Pulmonary Hypertension through Transforming Growth Factor-β–Smad Signaling. *American Journal of Respiratory Cell and Molecular Biology* 58: 194-207, 2018.
36. **Mandegar M, Fung YC, Huang W, Remillard CV, Rubin LJ, and Yuan JX**. Cellular and molecular mechanisms of pulmonary vascular remodeling: role in the development of pulmonary hypertension. *Microvasc Res* 68: 75-103, 2004.
37. **Marsboom G, Toth PT, Rya NJ, Hong Z, Wu X, Fang YH, Thenappan T, Piao L, Zhang HJ, Pogoriler J, Chen Y, Morrow E, Weir EK, Rehman J, and Archer SL**. Dynamin-Related Protein 1 (DRP1)-Mediated Mitochondrial Mitotic Fission Permits Hyperproliferation of Vascular Smooth Muscle Cells and Offers a Novel Therapeutic Target in Pulmonary Hypertension. *Circ Res* 110: 1484-1497, 2012.
38. **McLelland GL, Goiran T, Yi W, Dorval G, Chen CX, Lauinger ND, Krahn AI, Valimehr S, Rakovic A, Rouiller I, Durcan TM, Trempe JF, and Fon EA**. Mfn2 ubiquitination by PINK1/parkin gates the p97-dependent release of ER from mitochondria to drive mitophagy. *eLife* 7: 2018.
39. **Oka M, Homma N, Taraseviciene-Stewart L, Morris KG, Kraskauskas D, Burns N, Voelkel NF, and McMurtry IF**. Rho Kinase–Mediated Vasoconstriction Is Important in Severe Occlusive Pulmonary Arterial Hypertension in Rats. *Circulation Research* 100: 923-929, 2007.
40. **Orlova DY, Zimmerman N, Meehan S, Meehan C, Waters J, Ghosn EE, Filatenkov A, Kolyagin GA, Gernez Y, Tsuda S, Moore W, Moss RB, Herzenberg LA, and Walther G**. Earth Mover's Distance (EMD): A True Metric for Comparing Biomarker Expression Levels in Cell Populations. *PloS one* 11: e0151859, 2016.
41. **Ouellet M, Guillebaud G, Gervais V, Lupien St-Pierre D, and Germain M**. A novel algorithm identifies stress-induced alterations in mitochondrial connectivity and inner membrane structure from confocal images. *PLoS computational biology* 13: e1005612, 2017.
42. **Palmer CS, Osellame LD, Laine D, Koutsopoulos OS, Frazier AE, and Ryan MT**. MiD49 and MiD51, new components of the mitochondrial fission machinery. *EMBO Reports* 12: 565-573, 2011.

43. **Peng T-I, and Jou M-J**. Oxidative stress caused by mitochondrial calcium overload. *Ann N Y Acad Sci* 1201: 183-188, 2010.
44. **Picard M, Shirihai OS, Gentil BJ, and Burelle Y**. Mitochondrial morphology transitions and functions: implications for retrograde signaling? *American journal of physiology Regulatory, integrative and comparative physiology* 304: R393-406, 2013.
45. **R Development Core Team**. R: A Language and Environment for Statistical Computing. Vienna, Austria: 2018.
46. **Rabinovitch M**. Molecular pathogenesis of pulmonary arterial hypertension. *J Clin Invest* 122: 4306-4313, 2012.
47. **Rambold AS, Kostelecky B, Elia N, and Lippincott-Schwartz J**. Tubular network formation protects mitochondria from autophagosomal degradation during nutrient starvation. *Proceedings of the National Academy of Sciences* 108: 10190-10195, 2011.
48. **Rosca MG, Vazquez EJ, Chen Q, Kerner J, Kern TS, and Hoppel CL**. Oxidation of fatty acids is the source of increased mitochondrial reactive oxygen species production in kidney cortical tubules in early diabetes. *Diabetes* 61: 2074-2083, 2012.
49. **Ryan J, Dasgupta A, Huston J, Chen KH, and Archer SL**. Mitochondrial dynamics in pulmonary arterial hypertension. *Journal of molecular medicine (Berlin, Germany)* 93: 229-242, 2015.
50. **Sanders SP, Zweier JL, Kuppusamy P, Harrison SJ, Bassett DJ, Gabrielson EW, and Sylvester JT**. Hyperoxic sheep pulmonary microvascular endothelial cells generate free radicals via mitochondrial electron transport. *J Clin Invest* 91: 46-52, 1993.
51. **Scheraga RG, Abraham S, Niese KA, Southern BD, Grove LM, Hite RD, McDonald C, Hamilton TA, and Olman MA**. TRPV4 Mechanosensitive Ion Channel Regulates Lipopolysaccharide-Stimulated Macrophage Phagocytosis. *J Immunol* 196: 428-436, 2016.
52. **Seifert EL, Estey C, Xuan JY, and Harper ME**. Electron transport chain-dependent and -independent mechanisms of mitochondrial H2O2 emission during long-chain fatty acid oxidation. *J Biol Chem* 285: 5748-5758, 2010.
53. **Suresh K, Servinsky L, Jiang H, Bigham Z, Yun X, Kliment C, Huetsch JC, Damarla M, and Shimoda LA**. Reactive oxygen species induced Ca2+ influx via TRPV4 and microvascular endothelial dysfunction in the SU5416/Hypoxia model of pulmonary arterial hypertension. *Am J Physiol Lung Cell Mol Physiol* 2018.
54. **Suresh K, Servinsky L, Reyes J, Baksh S, Undem C, Caterina M, Pearse DB, and Shimoda LA**. Hydrogen peroxide-induced calcium influx in lung microvascular endothelial cells involves TRPV4. *Am J Physiol Lung Cell Mol Physiol* 309: L1467-1477, 2015.
55. **Suresh K, Servinsky L, Reyes J, Undem C, Zaldumbide J, Rentsendorj O, Modekurty S, Dodd-o JM, Scott AL, Pearse DB, and Shimoda LA**. CD36 mediates H2O2-induced calcium influx in lung microvascular endothelial cells. *American Journal of Physiology - Lung Cellular and Molecular Physiology* 2016.
56. **Suresh K, Servinsky L, Reyes J, Undem C, Zaldumbide J, Rentsendorj O, Modekurty S, Dodd OJ, Scott AL, Pearse DB, and Shimoda LA**. CD36 mediates H2O2-induced calcium influx in lung microvascular endothelial cells. *Am J Physiol Lung Cell Mol Physiol* ajplung 00361 02016, 2016.
57. **Suzuki T, Carrier EJ, Talati MH, Rathinasabapathy A, Chen X, Nishimura R, Tada Y, Tatsumi K, and West JD**. Isolation and characterization of endothelial-to-mesenchymal transition-cells in pulmonary arterial hypertension. *Am J Physiol Lung Cell Mol Physiol* ajplung 00296 02017, 2017.
58. **Szabadkai G, Simoni AM, Bianchi K, De Stefani D, Leo S, Wieckowski MR, and Rizzuto R**. Mitochondrial dynamics and Ca2+ signaling. *Biochimica et Biophysica Acta (BBA) - Molecular Cell Research* 1763: 442-449, 2006.
59. **Szarka N, Pabbidi MR, Amrein K, Czeiter E, Berta G, Pohoczky K, Helyes Z, Ungvari Z, Koller A, Buki A, and Toth P**. Traumatic brain injury impairs myogenic constriction of cerebral arteries: role of mitochondria-derived H2O2 and TRPV4-dependent activation of BKCa channels. *Journal of neurotrauma* 2017.
60. **Tang H, Babicheva A, McDermott KM, Gu Y, Ayon RJ, Song S, Wang Z, Gupta A, Zhou T, Sun X, Dash S, Wang Z, Balistrieri A, Zheng Q, Cordery AG, Desai AA, Rischard F, Khalpey Z, Wang J, Black SM, Garcia JGN, Makino A, and Yuan JX-J**. Endothelial HIF-2α contributes to severe pulmonary hypertension due to endothelial-to-mesenchymal transition. *American Journal of Physiology-Lung Cellular and Molecular Physiology* 314: L256-L275, 2018.
61. **Tang H, Yamamura A, Yamamura H, Song S, Fraidenburg DR, Chen J, Gu Y, Pohl NM, Zhou T, Jiménez-Pérez L, Ayon RJ, Desai AA, Goltzman D, Rischard F, Khalpey Z, Black SM, Garcia JGN, Makino A, and Yuan JXJ**. Pathogenic role of calcium-sensing receptors in the development and progression of pulmonary hypertension. *Am J Physiol Lung Cell Mol Physiol* 310: L846-859, 2016.

62. **Taraseviciene-Stewart L, Kasahara Y, Alger L, Hirth P, Mc Mahon G, Waltenberger J, Voelkel NF, and Tuder RM**. Inhibition of the VEGF receptor 2 combined with chronic hypoxia causes cell death-dependent pulmonary endothelial cell proliferation and severe pulmonary hypertension. *FASEB journal : official publication of the Federation of American Societies for Experimental Biology* 15: 427-438, 2001.

63. **Thorneloe KS, Cheung M, Bao W, Alsaid H, Lenhard S, Jian MY, Costell M, Maniscalco-Hauk K, Krawiec JA, Olzinski A, Gordon E, Lozinskaya I, Elefante L, Qin P, Matasic DS, James C, Tunstead J, Donovan B, Kallal L, Waszkiewicz A, Vaidya K, Davenport EA, Larkin J, Burgert M, Casillas LN, Marquis RW, Ye G, Eidam HS, Goodman KB, Toomey JR, Roethke TJ, Jucker BM, Schnackenberg CG, Townsley MI, Lepore JJ, and Willette RN**. An orally active TRPV4 channel blocker prevents and resolves pulmonary edema induced by heart failure. *Science translational medicine*\ 4\: 159ra148\.

64. **Tian L, Neuber-Hess M, Mewburn J, Dasgupta A, Dunham-Snary K, Wu D, Chen KH, Hong Z, Sharp WW, Kutty S, and Archer SL**. Ischemia-induced Drp1 and Fis1-mediated mitochondrial fission and right ventricular dysfunction in pulmonary hypertension. *Journal of molecular medicine (Berlin, Germany)* 95: 381-393, 2017.

65. **Touyz RM**. Reactive oxygen species as mediators of calcium signaling by angiotensin II: implications in vascular physiology and pathophysiology. *Antioxidants & redox signaling* 7: 1302-1314, 2005.

66. **Tsushima K, Bugger H, Wende AR, Soto J, Jenson GA, Tor AR, McGlauflin R, Kenny HC, Zhang Y, Souvenir R, Hu XX, Sloan CL, Pereira RO, Lira VA, Spitzer KW, Sharp TL, Shoghi KI, Sparagna GC, Rog-Zielinska EA, Kohl P, Khalimonchuk O, Schaffer JE, and Abel ED**. Mitochondrial Reactive Oxygen Species in Lipotoxic Hearts Induce Post-Translational Modifications of AKAP121, DRP1, and OPA1 That Promote Mitochondrial Fission. *Circ Res* 122: 58-73, 2018.

67. **Wakabayashi J, Zhang Z, Wakabayashi N, Tamura Y, Fukaya M, Kensler TW, Iijima M, and Sesaki H**. The dynamin-related GTPase Drp1 is required for embryonic and brain development in mice. *The Journal of cell biology* 186: 805-816, 2009.

68. **Wang W, Wang Y, Long J, Wang J, Haudek SB, Overbeek P, Chang BH, Schumacker PT, and Danesh FR**. Mitochondrial fission triggered by hyperglycemia is mediated by ROCK1 activation in podocytes and endothelial cells. *Cell metabolism* 15: 186-200, 2012.

69. **Wegierski T, Lewandrowski U, Muller B, Sickmann A, and Walz G**. Tyrosine phosphorylation modulates the activity of TRPV4 in response to defined stimuli. *The Journal of biological chemistry*\ 284\: 2923\, 2009.

70. **Weinberg F, Hamanaka R, Wheaton WW, Weinberg S, Joseph J, Lopez M, Kalyanaraman B, Mutlu GM, Budinger GR, and Chandel NS**. Mitochondrial metabolism and ROS generation are essential for Kras-mediated tumorigenicity. *Proceedings of the National Academy of Sciences of the United States of America* 107: 8788-8793, 2010.

71. **Xia Y, Fu Z, Hu J, Huang C, Paudel O, Cai S, Liedtke W, and Sham JS**. TRPV4 channel contributes to serotonin-induced pulmonary vasoconstriction and the enhanced vascular reactivity in chronic hypoxic pulmonary hypertension. *American journal of physiologyCell physiology*\ 305\: C704\, 2013.

72. **Xie Q, Wu Q, Horbinski CM, Flavahan WA, Yang K, Zhou W, Dombrowski SM, Huang Z, Fang X, Shi Y, Ferguson AN, Kashatus DF, Bao S, and Rich JN**. Mitochondrial control by DRP1 in brain tumor initiating cells. *Nature neuroscience* 18: 501-510, 2015.

73. **Xiong J, Kawagishi H, Yan Y, Liu J, Wells QS, Edmunds LR, Fergusson MM, Yu ZX, Rovira, II, Brittain EL, Wolfgang MJ, Jurczak MJ, Fessel JP, and Finkel T**. A Metabolic Basis for Endothelial-to-Mesenchymal Transition. *Molecular cell* 69: 689-698 e687, 2018.

74. **Xu H, Zhao H, Tian W, Yoshida K, Roullet JB, and Cohen DM**. Regulation of a transient receptor potential (TRP) channel by tyrosine phosphorylation. SRC family kinase-dependent tyrosine phosphorylation of TRPV4 on TYR-253 mediates its response to hypotonic stress. *The Journal of biological chemistry*\ 278\: 11520\, 2003.

75. **Xu W, and Erzurum SC**. Endothelial cell energy metabolism, proliferation, and apoptosis in pulmonary hypertension. *Compr Physiol* 1: 357-372, 2011.

76. **Xu W, Kaneko FT, Zheng S, Comhair SAA, Janocha AJ, Goggans T, Thunnissen FBJM, Farver C, Hazen SL, Jennings C, Dweik RA, Arroliga AC, and Erzurum SC**. Increased arginase II and decreased NO synthesis in endothelial cells of patients with pulmonary arterial hypertension. *FASEB journal : official publication of the Federation of American Societies for Experimental Biology* 18: 1746-1748, 2004.

77. **Xu W, Koeck T, Lara AR, Neumann D, DiFilippo FP, Koo M, Janocha AJ, Masri FA, Arroliga AC, Jennings C, Dweik RA, Tuder RM, Stuehr DJ, and Erzurum SC**. Alterations of cellular bioenergetics in pulmonary artery endothelial cells. *Proceedings of the National Academy of Sciences of the United States of America* 104: 1342-1347, 2007.

751 78. **Yu T, Robotham JL, and Yoon Y**. Increased production of reactive oxygen species in hyperglycemic conditions
752 requires dynamic change of mitochondrial morphology. *Proceedings of the National Academy of Sciences of the United*
753 *States of America* 103: 2653-2658, 2006.
754 79. **Zecchin A, Kalucka J, Dubois C, and Carmeliet P**. How Endothelial Cells Adapt Their Metabolism to Form Vessels
755 in Tumors. *Frontiers in Immunology* 8: 2017.

756

757

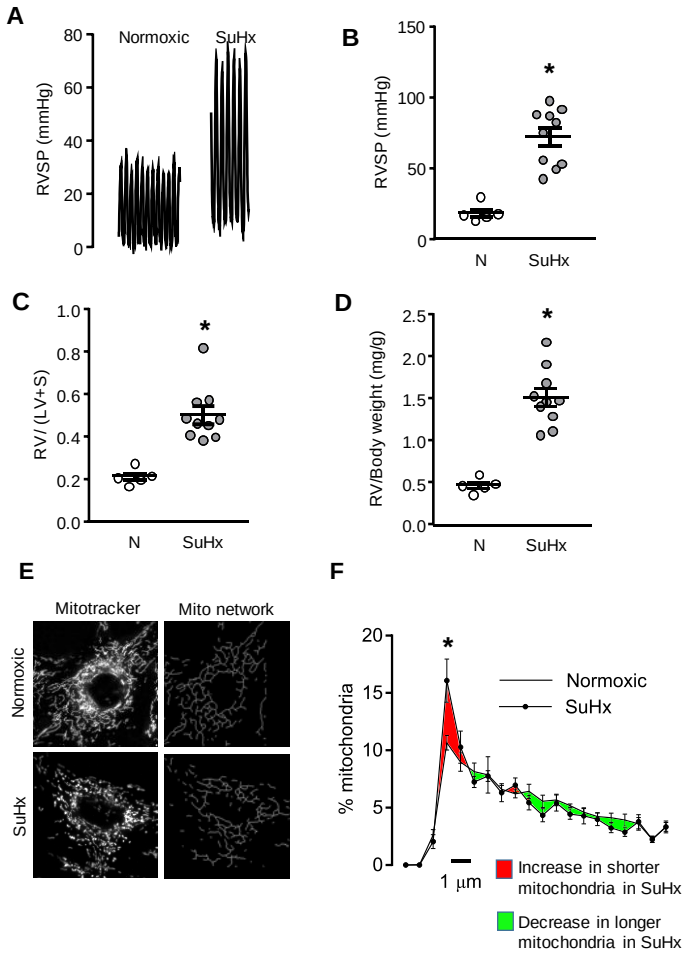

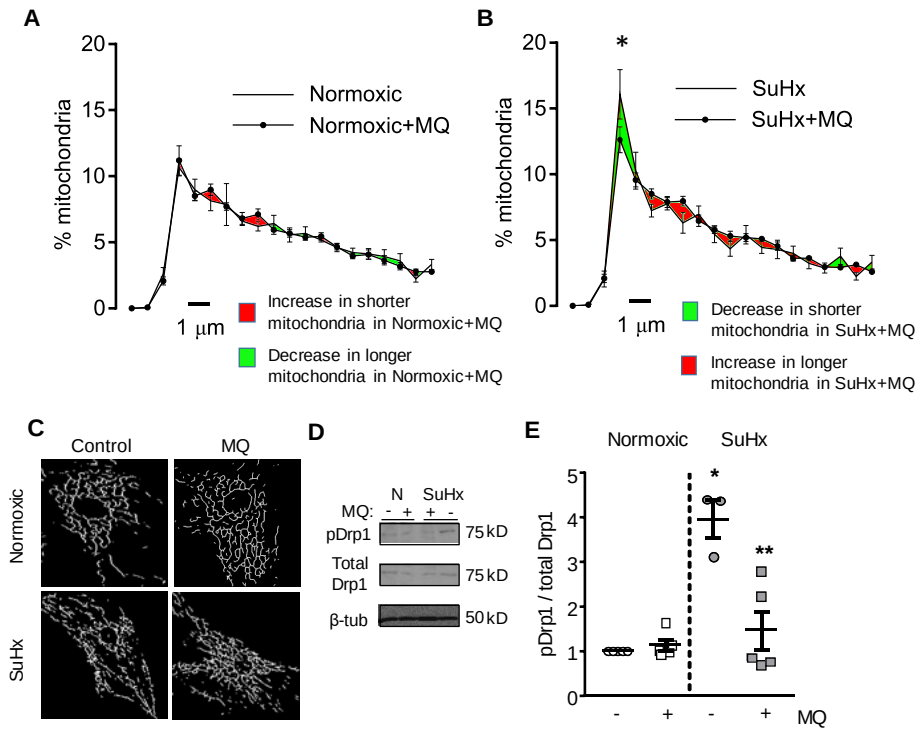

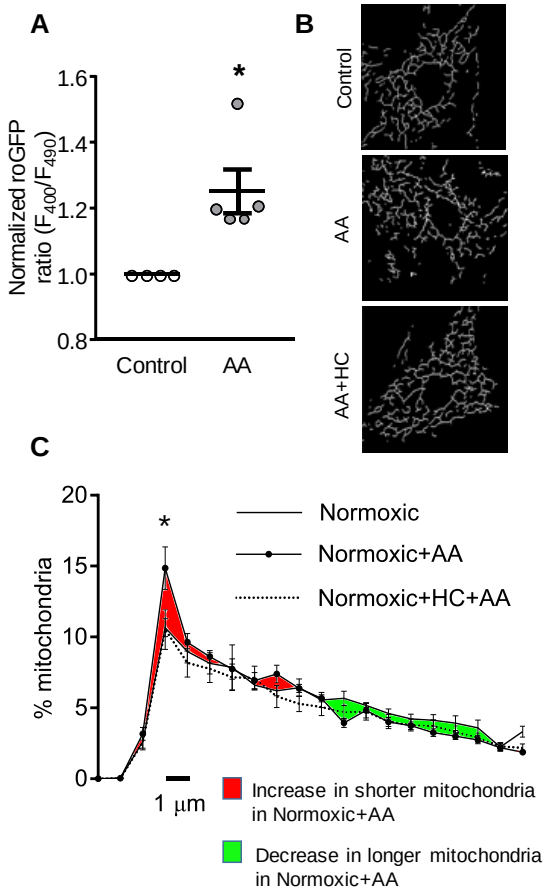

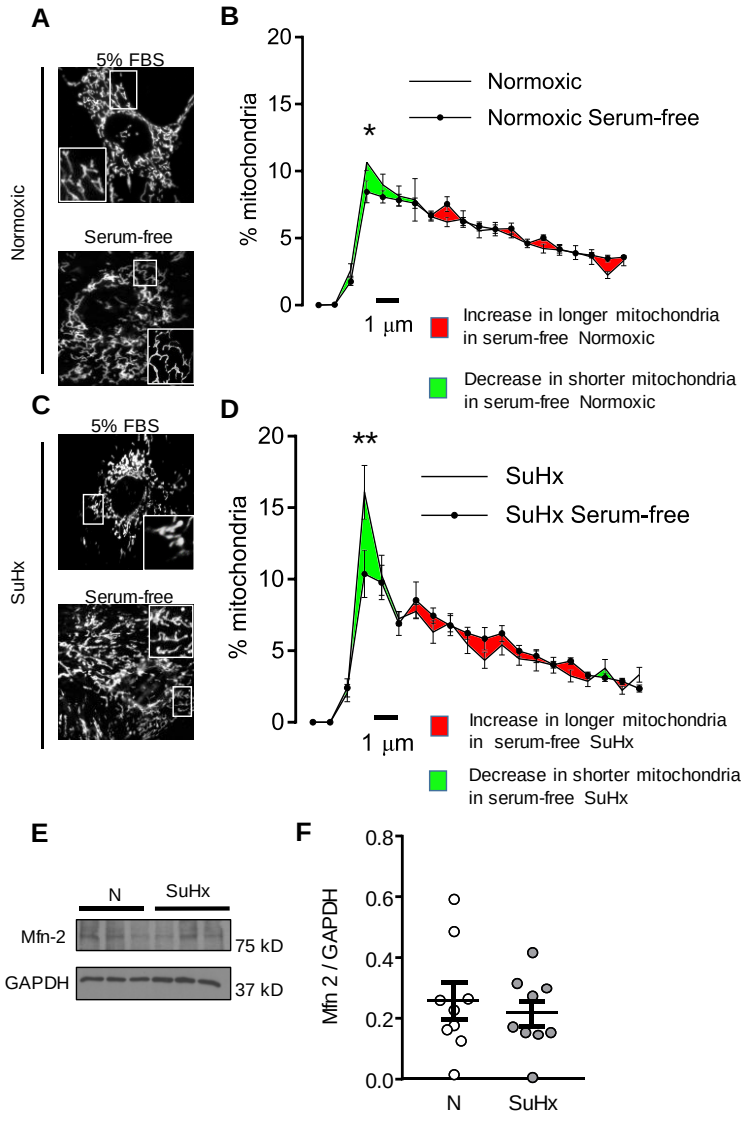

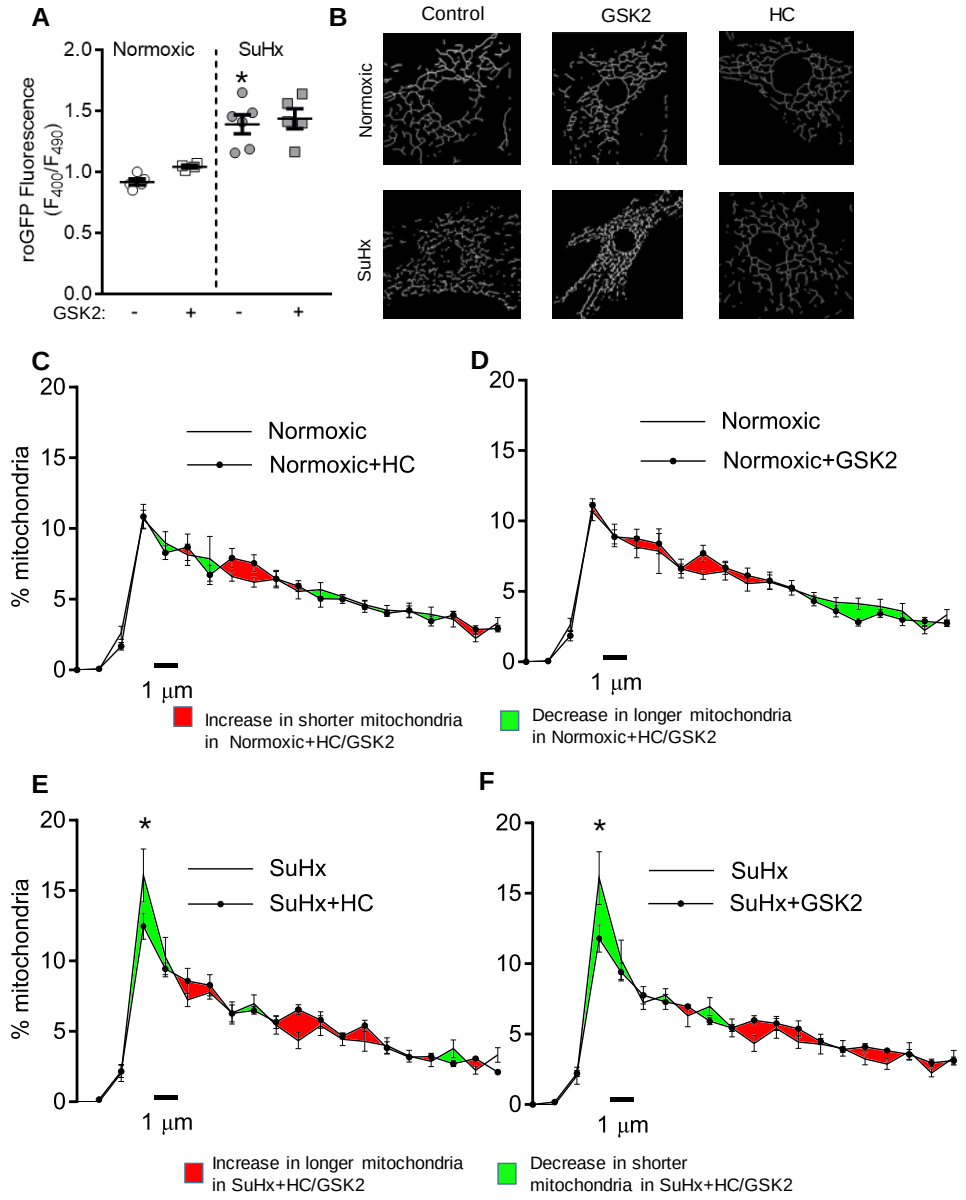

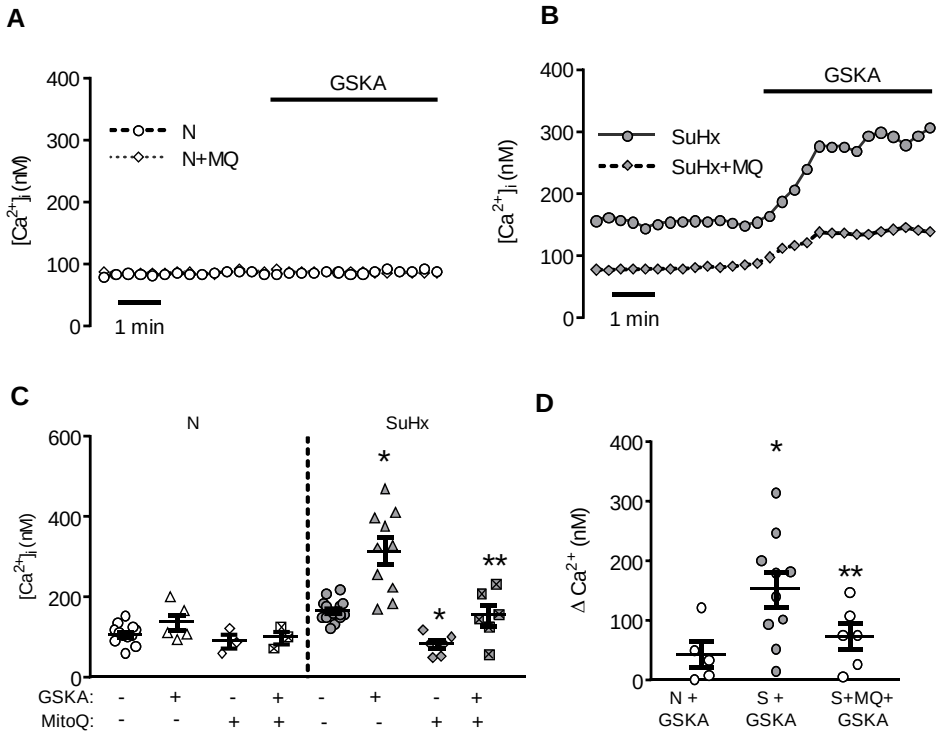

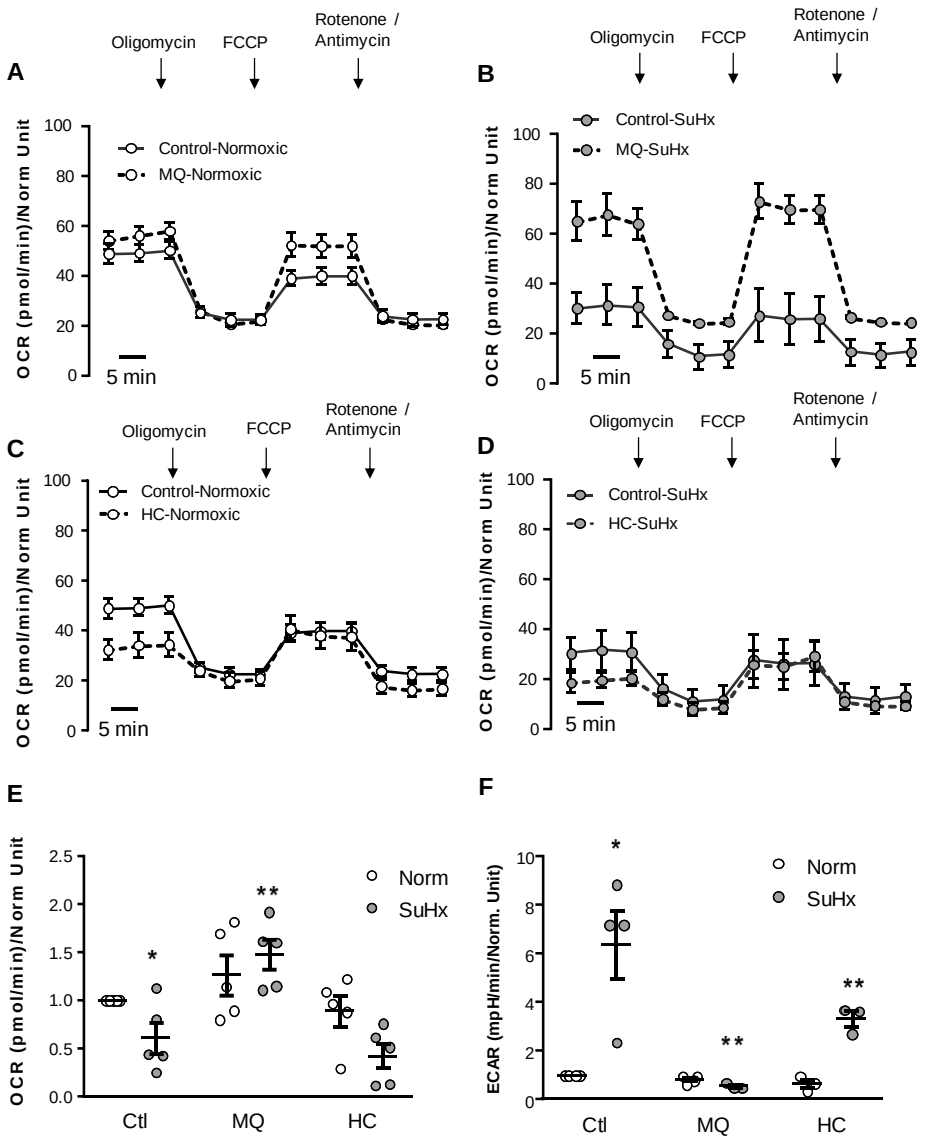

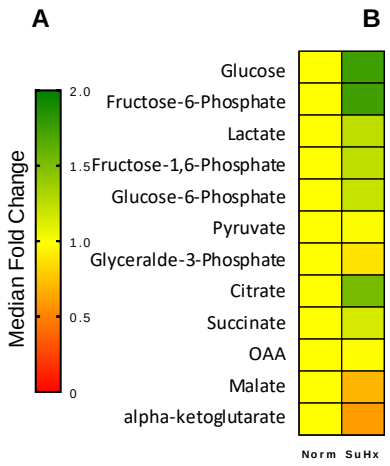

B

Metabolite	Median Fold Change	IQR	p
Glucose	1.752	(1.12,2.12)	0.07
Fructose-6-Phosphate	1.743	(1.08,2.37)	0.06
Lactate	1.254	(0.83, 1.57)	0.14
Fructose-1,6-Phosphate	1.248	(0.66,9.89)	0.312
Glucose-6-Phosphate	1.22	(0.96,1.61)	0.007
Pyruvate	1.015	(0.87, 1.65)	0.28
Glyceralde-3-Phosphate	0.89	(0.27,6.81)	0.81
Citrate	1.535	(0.86,3.02)	0.07
Succinate	1.161	(0.85,2.51)	0.38
OAA	0.99	(0.74,2)	0.84
Malate	0.71	(0.56,1.24)	0.54
alpha-ketoglutarate	0.61	(0.25,1.53)	0.81